Infrared Physics & Technology 133 (2023) 104821

Contents lists available at ScienceDirect

Infrared Physics and Technology

journal homepage: www.elsevier.com/locate/infrared

Regular article

Enhancing long-term stability of photoacoustic gas sensor using an extremum-seeking control algorithm

Anastasia Bednyakova [a,*], Evgenii Erushin [a,b,c], Ilya Miroshnichenko [b,c], Nadezhda Kostyukova [a,b,c], Andrey Boyko [a,b], Alexey Redyuk [a]

[a] Novosibirsk State University, Pirogova str. 2, Novosibirsk 630090, Russia
[b] Institute of Laser Physics SB RAS, Lavrentyev av. 15b, Novosibirsk 630090, Russia
[c] Novosibirsk State Technical University, K. Marksa av. 20, Novosibirsk 630073, Russia

ARTICLE INFO

Keywords:
Gas sensing
Gas analysis
Photoacoustics
Absorption
Spectroscopy
Long-term stability
Resonator frequency drift
Concentration methane monitoring
Extremum-seeking control
Optimization algorithm

ABSTRACT

Smart sensor systems have gained increasing importance in various fields, including healthcare, environmental monitoring, industrial automation, and security. Photoacoustic gas sensors are an emerging type of optical sensor used in various applications due to its enhanced performance characteristics. However, the accuracy and reliability of gas concentration measurements from photoacoustic gas sensors may be impacted by several known limitations, including drift of the gas cell resonant frequency over extended periods of time. Researchers have proposed various solutions, including optimization methods and signal processing algorithms, to address this and others issues. In this paper, we propose a novel solution using an extremum-seeking control algorithm to manage the laser modulation frequency of photoacoustic gas sensors. By tracking the changing resonant frequency of the gas cell, long-term stability can be achieved, making it suitable for environmental monitoring, petroleum exploration, and industrial process control. Our approach has the potential to improve the accuracy and reliability of long-term measurements obtained from photoacoustic gas sensors, providing a stable and reliable method for gas concentration estimation.

1. Introduction

Smart sensors and sensor systems are emerging technologies that have become increasingly important in everyday life over the last decade with applications in a wide range of fields such as healthcare, environmental monitoring, industrial automation, security, and more. Sensors are devices that can detect characteristics of physical, chemical, and biological processes and convert them into signals that can be analyzed and interpreted. They provide real-time and continuous data about the state of the environment or the system being monitored, enabling timely and accurate decision making.

There are various types of sensors, including temperature, pressure, humidity, and gas sensors. Optical gas sensors, in particular, have gained increasing attention in recent years due to their advantages such as high sensitivity, selectivity, and stability [1]. They can be further classified into different types based on the physical phenomenon they exploit, including absorption, fluorescence, and photoacoustic phenomena. Photoacoustic gas sensor (PAGS) is a type of optical sensors that measures gas concentration based on the absorption of light by gas molecules, resulting in a local temperature increase and the emission of acoustic waves [2]. Nowadays PAGS have been widely used in environmental monitoring, industrial process control, and medical diagnosis due to their improved performance characteristics. In environmental monitoring, PAGS are used to measure greenhouse gases such as methane and carbon dioxide [3]. In industrial process control, they are used for gas detection and monitoring of combustion processes [4]. In medical diagnosis, PAGS can be used for breath analysis to detect diseases such as lung cancer [5].

A crucial component of optical gas sensors is the radiation source as it determines the spectral range of the device. There are different types of radiation sources that can be used for PAGS, including non-coherent sources like LEDs and mid-infrared lamps, as well as coherent sources such as optical parametric oscillators (OPOs), quantum cascade lasers (QCLs), discretely tunable solid-state and gas lasers [6]. The use of OPOs and QCLs offers the advantage of continuous tuning of the radiation wavelength. OPOs, in particular, provide the ability to change the wavelength in a wide range of up to tens of micrometers within a single device [7,8]. The OPO operation is based on frequency down-conversion in a nonlinear crystal, as a result of which monochromatic pump radiation is converted into tunable radiation of signal and idler

* Corresponding author.
E-mail address: anastasia.bednyakova@gmail.com (A. Bednyakova).

https://doi.org/10.1016/j.infrared.2023.104821
Received 19 May 2023; Received in revised form 7 July 2023; Accepted 7 July 2023
Available online 13 July 2023
1350-4495/© 2023 Elsevier B.V. All rights reserved.

waves. By employing widely tunable OPOs in PAGS, it becomes possible to detect multiple gases simultaneously, thus enhancing the universality of this approach [9]. To minimize the effect of cross-sensitivity in multi-component gas analyzers, various mathematical analysis methods can be applied, such as canonical correlation analysis [10], principal component analysis [5], and others.

However, photoacoustic gas sensors have several known limitations, such as gas cell resonant frequency drift, sensitivity to external disturbances, and cross-sensitivity to other gases [2,11]. A particularly significant drawback is the drift of the resonant frequency of the gas cell. The operation of the sensor relies on the alignment between the repetition rate of laser pulses propagating through the gas being studied and the resonant frequency of the gas cell. When the resonant frequency of the gas cell fluctuates due to temperature changes or other external factors, a tool to control and adjust the laser modulation frequency is necessary. All these limitations can affect the accuracy and reliability of gas concentration measurements, particularly over extended periods of time. Researchers, motivated by the need to improve long-term stability of PAGS, have proposed various solutions, such as using reference cells, temperature stabilization and signal processing algorithms [12].

With the increased use of sensors in recent times, sensor systems generate a large amount of data that must be collected, analyzed and interpreted. As a result, optimization and machine learning methods have been applied to sensor systems to manage their performance, control their operating conditions, and process gathered information. These methods are useful in improving the accuracy, efficiency, and robustness of the sensor systems. They can help to adapt to changing environmental conditions, reduce noise and interference, and handle large amounts of data. One of the such optimization methods is the extremum-seeking control algorithm (ESCA). ESCA is a closed-loop control strategy that can optimize the performance of a system by seeking the extremum of a cost function [13,14]. By adjusting the system's input parameters, the algorithm can find the optimal operating conditions that minimize the cost function. ESCA has been used in various applications, including robotics, process control, and environmental monitoring [15–17].

In this paper, we present a novel solution to address the drift in the resonant frequency of a gas cell observed in PAGS. Specifically, we propose the use of an extremum-seeking control algorithm to manage the radiation source pulse repetition rate and make it follow the resonant frequency of the gas cell, thereby achieving long-term stability of a gas sensor. We demonstrate the effectiveness of the proposed algorithm through experiments and estimate its performance. Our results show that the ESCA can effectively maintain the stability of the PAGS over extended periods, making it suitable for various applications, including environmental monitoring, petroleum exploration, and industrial process control. By providing a solution for real-time tracking the resonant frequency of the gas cell, our proposed approach has the potential to significantly improve the accuracy and reliability of long-term gas concentration measurements obtained from PAGS.

2. Experimental setup

The key components of PAGS include a radiation source emitting at a wavelength that matches the absorption line of the gas being investigated, a gas cell that serves as a resonator, and a detector that captures the acoustic signal produced when the radiation interacts with the gas. To enable continuous wavelength tuning, we utilized an optical parametric oscillator as the radiation source, as depicted in Fig. 1. The developed OPO enables continuous tuning of the wavelength within the range of 2.5–4.5 μm and can be used for multi-component gas analysis, for example, for water vapor, acetone, hydrocarbons, and CO_2 isotopes detection. For this experimental study, the wavelength of the OPO radiation was set to match the maximum absorption peak of methane at approximately 3.32 μm. The OPO pump source was a diode-pumped Q-switched Nd:YLF laser (TECH-1053 Advanced, Laser-export

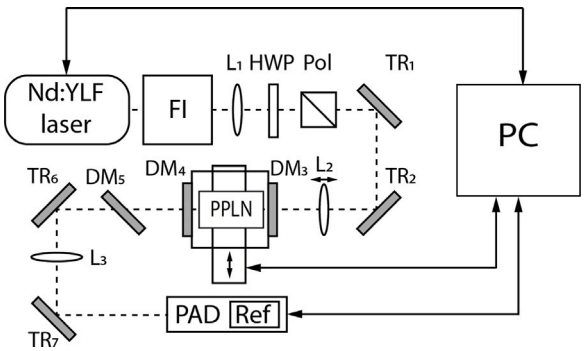

Fig. 1. The experimental setup of the developed PAGS system: FI — Faraday isolator, L_1 and L_2 — lenses, HWP — half-wave plate, Pol — polarizer, TR — total reflected mirrors, DM — dichroic mirrors, PAD — photoacoustic detector, Ref — non-resonant reference cell, PPLN — fan-out periodically poled lithium niobate crystal, PC — personal computer.

Co. Ltd.) that produced pulses with a duration of 6 ns and energy up to 1 mJ at 1.053 μm. The radiation linewidth was 227 pm (approximately 2 cm^{-1}), and the beam quality factor M^2 was around 1.4. The pulse repetition rate could be varied from 0.1 to 4 kHz. To prevent feedback from optical elements, we employed a Faraday isolator (FI). For smooth power control, a half-wave plate (HWP) with a Glan prism (Pol) was applied. We used the lens L_1 with a focal length of 300 mm to match the modes of the pump laser and the OPO cavity.

A differential photoacoustic detector (PAD) based on a resonator with a fundamental resonance frequency of approximately 1750 Hz and a Q-factor of around 40 was employed as the gas detector. The detector geometry is identical to that of the cell which was previously described in detail in [18]. It is constructed from a solid aluminum alloy and comprise two parallel acoustic channels with dimensions of $Ø9 \times 90$ mm separated by a thin 1 mm partition, as well as two buffer cavities ($Ø20 \times 8$ mm) that are closed by flanges with rubber seals. To minimize optical losses, ZnSe Brewster windows were installed at both flanges. The gas was pumped through hoses mounted on the walls of the buffer cavities.

In the middle of each acoustic resonator of the differential PAD, two microphones are installed and connected to a differential amplifier. To measure the current lowest resonant frequency, a piezoelectric sound emitter is positioned in the center of one of the acoustic resonators. This emitter acts as a speaker, generating acoustic vibrations within the PAD. The resonant frequency is then measured when the PAD is filled with air or nitrogen, which is approximately 1750 Hz and 1780 Hz, respectively. Modulating the laser at this frequency results in a maximum PAD signal. The technique for measuring the resonant frequency of the PAD is described in detail in [18]. The PAD comprises two cells: a resonant cell and a non-resonant reference (REF) cell. The REF cell is filled with a gas mixture of known concentration, in this case, methane in nitrogen (1% $CH_4 + N_2$), and serves to compensate for the impact of wavelength and power drift of the OPO on the PAD signal. The signals from the cells are transformed into the frequency domain using Fast Fourier Transform from digitized signals captured by cell microphones. The Fourier bin corresponding to the resonant frequency of the resonant cell is identified, and the amplitude of the signal in that bin is determined. The PAD signal is calculated by taking the ratio of the amplitude of the resonant cell Fourier bin to the amplitude of the REF cell calculated in the same Fourier bin. To evaluate the algorithm's performance, the PAD was filled with a test gas mixture containing 9.7 ppm of methane in nitrogen, which is approximately five times higher than the background concentration of methane in air.

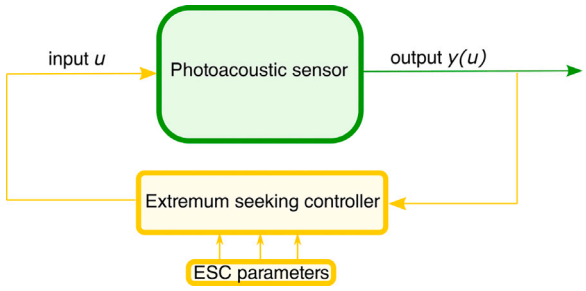

Fig. 2. Schematic depiction of the feedback loop for the photoacoustic gas sensor.

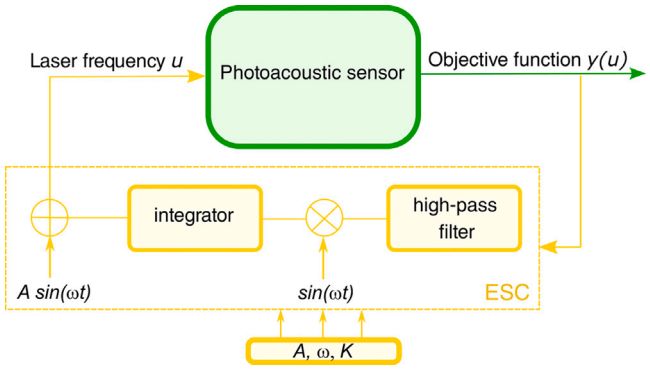

Fig. 3. Scheme of the extremum-seeking controller.

2.1. PPLN OPO

The nonlinear medium of the OPO used to generate radiation in the spectral region of 2.5–4.5 μm was a fan-out MgO:PPLN structure (50 × 20 × 3 mm, Labfer Ltd.). The domain structure's period varied smoothly along the y-axis in the range of Λ=27.5–32.5 μm. To minimize optical losses within the OPO cavity, the crystal faces were antireflection-coated at around 1.5 μm. A thermostat housed on a motorized translation stage was used to maintain the crystal temperature at 40 °C.

Two metallic totally reflected mirrors TR_1 and TR_2 were used to introduce the laser beam into the OPO cavity. To achieve the desired beam size in the crystal, a lens L_2 with a focal length of f=200 mm was used, resulting in a size of $d_{x,y} \approx 290$ μm (at a level of e^{-2}). In contrast to [19], a single-pass optical parametric oscillator was used in this study. The cavity was formed by two flat dichroic mirrors, DM_3 and DM_4, which are transparent to pump and idler waves, but totally reflected the signal wave. These mirrors were installed in the monolith cube close to the edge of MgO: PPLN (with a gap of ~0.5 mm on each side).

Tuning of the OPO was achieved by shifting the structure along the axis of the optical cavity using a motorized translation stage with a 25 mm travel range and 1.25 μm resolutions in full step. Tuning data was recorded in a calibration file for further measurements, with an accuracy of setting the specified wavelength at ±0.1 nm. The linewidth of the PPLN OPO emission was measured to be ~ 5.6 ± 0.2 cm^{-1} at 3312 nm and ~ 5.5 ± 0.5 cm^{-1} over the entire tuning range. The OPO radiation wavelength and linewidth were measured using a High Finesse spectrometer (LSA IR-I) with a resolution of 12 GHz (~50 pm). The average OPO output power for methane detection was ~35 mW.

2.2. Realization of feedback loop

The resonant frequency of the photoacoustic cell may change over time, for example, as a result of changes in the ambient temperature or the temperature of the gas mixture inside the cell. This effect is negative, since in order to accurately determine the gas concentration, the repetition rate of laser pulses must correspond to the resonant frequency of the cell at each moment of time. To adjust the repetition rate of the laser pulses, a feedback loop was implemented in the system (Fig. 2). The input signal for the sensor is the time-controlled frequency of the laser pulses $u(t)$, the output signal is the value of the objective function $y(u(t))$, which definition is given in the next section. We use extremum-seeking control algorithm to control the $u(t)$ variation in time.

3. Extremum-seeking controller

The extremum-seeking control algorithm is a model-free adaptive control algorithm that finds and tracks the local maxima of the objective function by changing the input parameters [14–17]. It is useful for optimizing parameters to unknown dynamics of complex nonlinear

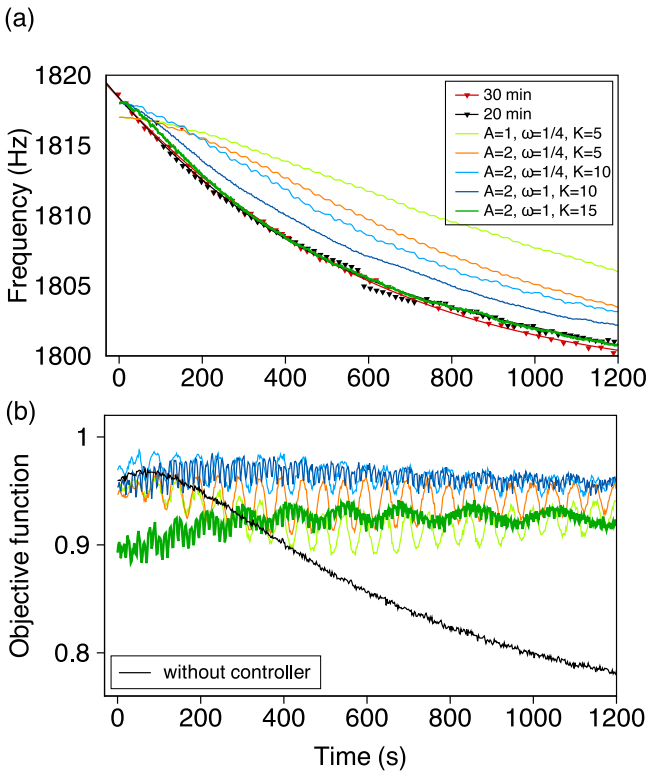

Fig. 4. Temporal evolution of the laser modulation frequency (a) and objective function (b) measured at different values of ESCA parameters. Black and red triangles show PAD resonant frequency measured by the speaker under similar conditions for 20 and 30 min correspondingly.

systems in real time. At the first stage of ESCA low-amplitude sinusoidal modulation is added to the input signal. System reacts to the parameter perturbations, which causes a corresponding change in the objective function value. Then the measured variation in the objective function is compared with the varying input signal to dynamically improve an estimate of the optimal input parameter.

Fig. 3 shows an algorithm diagram for a sensor system with one input and one output. The input variable u is the repetition rate of the laser pulses, the output variable is the value of the objective function $y(u)$. The objective function is defined as the value of the PAD signal, equal to the resonant cell signal normalized by REF signal. The procedure used to calculate the PAD signal is described in the Experimental Setup section. As previously mentioned, the use of a reference cell enables compensation for any drift in the power and wavelength of the OPO radiation. The algorithm starts working with adding a sinusoidal modulation $Asin(\omega t)$ to the best guess of the input $\hat{u}$ that maximizes

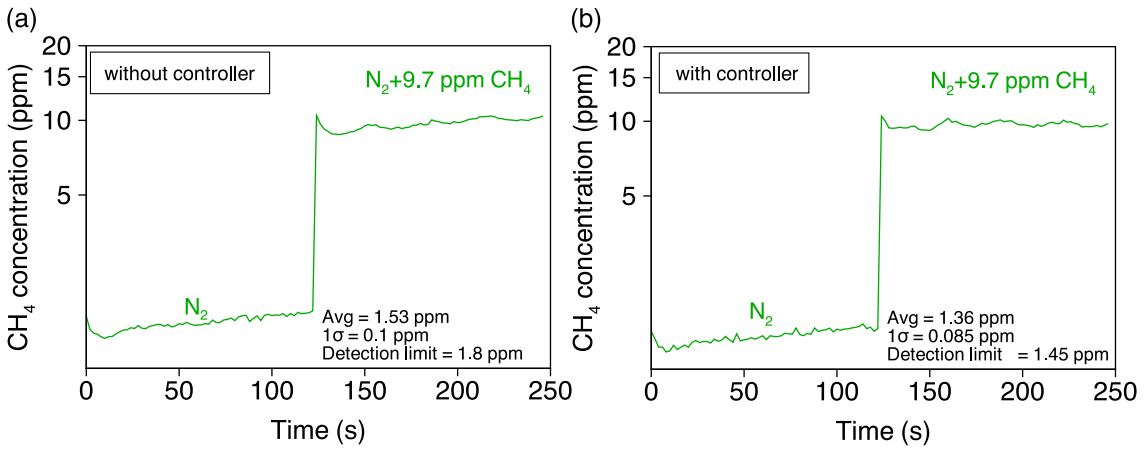

Fig. 5. Experimental recordings of normalized responses of PAD without and with ESCA when it is filled with N_2 and N_2 + 9.7 ppm CH_4 test gas mixture.

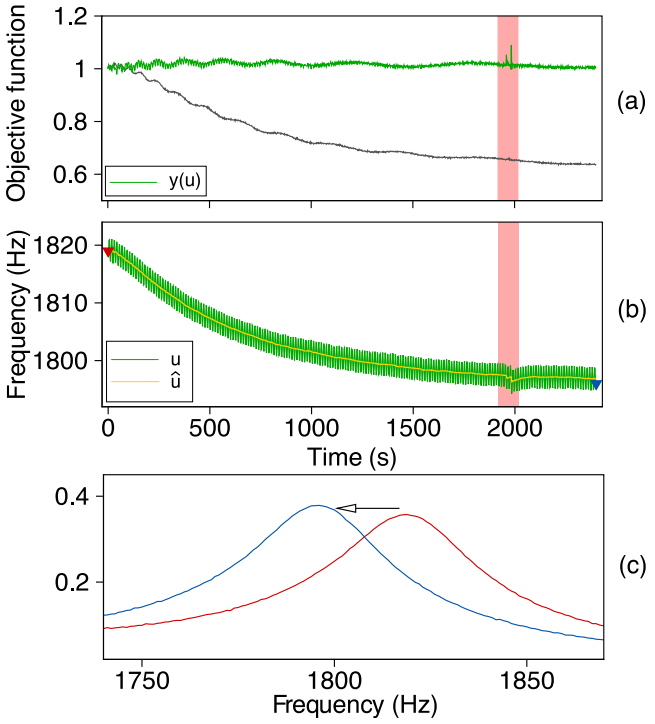

Fig. 6. 40-minute test of the algorithm performance during PAD cooling from ~37 °C to room temperature: (a) evolution of the objective function without (gray line) and with (green line) ESCA; (b) variation of the laser modulation frequency over time. Red and blue triangles show the measured PAD resonant frequency; (c) corresponding shift of the resonance peak during the experiment.

the objective function. This perturbation passes through the system, resulting in a perturbation of the objective function $y(u)$. The objective function is then multiplied by a high-pass filter to remove bias from the signal. Next, we obtain a demodulated signal by multiplying the filtered objective function signal by a sinusoid $sin(\omega t)$ with the same frequency as the modulation signal. Finally, we update the value of the estimate $\hat{u}$ by integrating the demodulated signal, which brings $\hat{u}$ closer to the local maximum. Our implementation of the algorithm was inspired by demo code intended as a companion to the book [20].

4. Results and discussion

In order to ensure stable algorithm operation, it is necessary to select appropriate values for certain parameters. In this study, we focused on optimizing the amplitude of the sinusoidal modulation A, the modulation frequency ω, and the integrator gain K. Fig. 4 illustrates how the choice of these parameters impacts algorithm convergence. We heated the PAD to a temperature of ~37 °C and allowed it to cool for 20 min to ~25 °C with the controller engaged. It should be noted that the temperature sensor was placed on the PAD housing. The black and red triangles shown in Fig. 4a represent the PAD resonant frequency drift measured by the speaker during the cell cooling process. The colored lines in Fig. 4 depict the changes in laser modulation frequency and corresponding behavior of the objective function during algorithm execution.

It is worth noting that perturbation frequency is limited by the frequency of the measuring equipment ω_p. In the following discussion, we will refer to ω as the dimensionless quantity representing the ratio of the perturbation frequency to the maximum achievable frequency. A larger value of ω leads to faster convergence, as demonstrated by the comparison of the light blue and dark blue lines in Fig. 4, as well as better sensitivity to environmental changes. Increasing the modulation amplitude A leads to faster algorithm convergence, as shown in Fig. 4a, but also results in more oscillations of the objective function around the optimum, as demonstrated in Fig. 4b. Similarly, increasing the integrator gain K also results in faster convergence, but when K exceeds 15, the laser modulation frequency begins to oscillate significantly and deviate from the optimal trajectory. We assume that the origin of the low-frequency modulation of the objective function, clearly visible on the dark green line in Fig. 4b, is related to the laser power and wavelength drift which was not fully compensated by REF signal normalization or to the spatial drift of the OPO beam in PAD. Therefore, based on the aforementioned considerations, we select the parameter values A=2, ω=1, and K=15 as optimal and utilize them throughout the paper.

To study the impact of ESCA on sensitivity and detection limits, the PAD was alternately filled with dry nitrogen and a mixture of reference gases, consisting of nitrogen mixed with methane (N_2 + 9.7 ppm CH_4). All methane detection measurements were performed at room temperature and atmospheric pressure, using a wavelength of 3.313 μm and a pulse repetition rate of 1798 Hz. Fig. 5 shows the experimental records of the normalized PAD response, both with and without ESCA. The response was calibrated using the known concentration of methane in the gas mixture under investigation (9.7 ppm). The limit of CH_4 detection (μ+3σ) [21] without and with ESCA was ~1.8 ppm and ~1.6 ppm, respectively. It is important to note that our study did not aim to achieve the lowest possible sensitivity, so all measurements were carried out at less than the maximum OPO energy. ESCA did not affect the limit of detection, however, it significantly improved the long-term stability of the measurements, as demonstrated below.

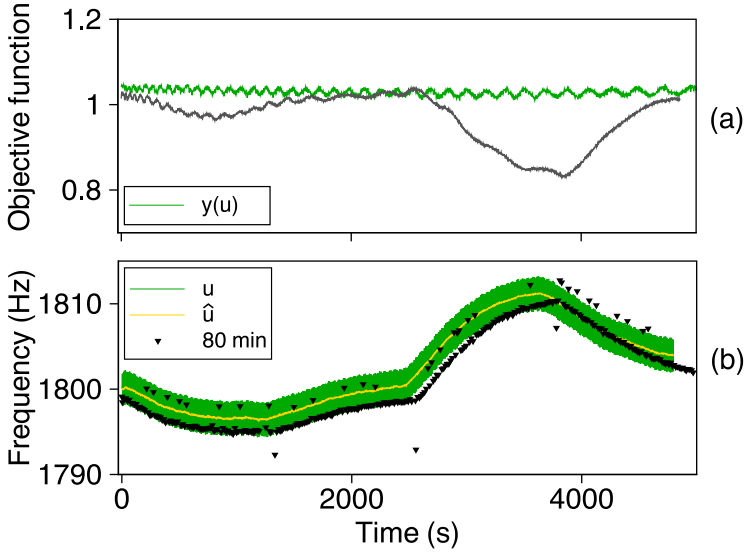

Fig. 7. 80-minute test of the algorithm performance under PAD temperature changes: (a) evolution of objective function without (gray line) and with (green line) ESCA; (b) variation of the PAD resonant frequency over time (black triangles) and adjustment of the laser pulse repetition rate.

Fig. 6 illustrates the results of the algorithm's execution when the gas cell was initially heated to ~37 °C and then allowed to cool down for 40 min to room temperature (~25 °C). The ESCA controller stabilized the objective function at the highest constant level, as shown by the green line in Fig. 6a. Please note that the spikes observed in the objective function (as indicated by the pink rectangles) were caused by a random external disturbance, which occurred due to a post falling onto the optical table. Even this external disturbance did not cause a malfunction in the algorithm. In contrast, without the controller, the value of the objective function decreased by 40% from the maximum value (gray line in Fig. 6a). The corresponding change in laser modulation frequency is shown in Fig. 6b. As it was not possible to measure the resonant frequency of the cell directly using a speaker during the algorithm execution, we measured the frequency before and after the sensor's operation. The initial frequency is marked with a red triangle, and the final frequency is marked with a blue triangle. The shift of the resonance peak in the Fourier space is shown in Fig. 6c.

We also investigated how a sinusoidal temperature variation combining cooling and heating of the cell affects the performance of the algorithm. The results of the experiment, which lasted for 80 min (corresponding to one period of the sinusoid), are shown in Fig. 7. When the controller is enabled, the objective function value remains close to the constant, while without the controller, it deviates from the maximum (compare the green and gray lines in Fig. 7a). The repetition rate of the laser pulses tracks changes in temperature. Black triangles demonstrates the variation of the gas cell resonant frequency with time, which was directly measured by the speaker under similar conditions of sinusoidal temperature variation (Fig. 7b).

The test measurements conducted above demonstrate that using ESCA for PAGS improves the long-term stability of gas concentration measurements. However, one drawback and constraint of the proposed method is the requirement for manual adjustment of the algorithm coefficients, namely A, ω, and K. To overcome this limitation we plan to improve the algorithm to automatically search for suitable coefficients. Additionally, this approach can be extended to monitor concentrations of other gases that absorb in the mid-IR range. For this purpose, radiation sources with wavelengths corresponding to the absorption line of the target gas should be utilized, and the REF cell of the gas mixture should contain a fixed concentration of the investigated substance to offset wavelength and radiation power level drift. Furthermore, the method can be adapted for use in multi-component gas sensors. In this case, the REF cell should contain mixtures of target gases with fixed concentrations, and the absorption lines of the selected gases must be spectrally separated. As for the necessary hardware equipment, a minor disadvantage of the proposed method is the accuracy of setting the laser pulse repetition frequency, which is limited by the microcontroller capabilities. The current experimental setup allows setting the frequency with an accuracy of approximately 0.1 Hz for frequencies around 1700 Hz, which may affect the algorithm performance. To assess the effect of this issue, additional experiments with variable frequency are required.

5. Conclusions

Today, a wide range of problems require accurate measurement of low gas concentrations over extended periods, ranging from ten minutes to several hours. Examples include terrain mapping to search for oil and gas deposits, as well as long-term monitoring of exhaled air to detect diseases. In addition, the monitoring of gas concentrations is crucial to ensure safety in industries, particularly in boiler rooms and gas-fired power stations. To address this challenge, we have proposed a new solution based on the extremum-seeking control algorithm, which ensures the long-term stability of photoacoustic gas sensors. Our solution is based on the principle of automatically searching for the optimal laser modulation frequency to compensate for changes in the resonant frequency of the gas cell, which enables us to measure gas concentrations more accurately. We experimentally demonstrated the effectiveness of our algorithmic approach in measuring methane concentration and maintaining sensor stability. Furthermore, we tested the performance of our method on mitigating the impact of significant changes in the resonant frequency caused by sharp changes in external temperature. The proposed approach can be applied for the long-term monitoring of concentrations of various biomarkers, industrial gases, and major greenhouse gases such as carbon dioxide isotopes, ammonia, nitrogen monoxide, and acetone, etc. Additionally, it can be adapted to other photoacoustic gas sensor configurations that use different radiation sources.

Declaration of competing interest

The authors declare the following financial interests/personal relationships which may be considered as potential competing interests:

Anastasia Bednyakova, Alexey Redyuk reports financial support was provided by Ministry of Science and Higher Education of the Russian Federation. Nadezhda Kostyukova, Andrey Boyko, Evgenii Erushin reports financial support was provided by Russian Science Foundation.

Data availability

Data will be made available on request.

Acknowledgments

This paper is dedicated to the memory of our dear colleague Dmitry Kolker who sadly passed away last year. He made an essential contribution to the development of optical parametric oscillators for gas analytical systems.

Funding

This research was funded by the Ministry of Science and Higher Education of the Russian Federation (Project No. FSUS-2021-0015). Experiments to study the dependence of the PAD resonant frequency on temperature were carried out with financial support from the Russian Science Foundation (Project 17-72-30006).

References

[1] J. Hodgkinson, R.P. Tatam, Optical gas sensing: a review, Meas. Sci. Technol. 24 (1) (2012) 012004, http://dx.doi.org/10.1088/0957-0233/24/1/012004.

[2] S. Palzer, Photoacoustic-based gas sensing: A review, Sensors 20 (9) (2020) http://dx.doi.org/10.3390/s20092745, URL https://www.mdpi.com/1424-8220/20/9/2745.

[3] A. Ngai, S. Persijn, G. von Basum, F. Harren, Automatically tunable continuous-wave optical parametric oscillator for high-resolution spectroscopy and sensitive trace-gas detection, Appl. Phys. B 85 (2006) 173–180, http://dx.doi.org/10.1007/s00340-006-2362-3, URL https://link.springer.com/article/10.1007/s00340-006-2362-3.

[4] S. Schilt, L. Thévenaz, M. Niklès, L. Emmenegger, C. Hüglin, Ammonia monitoring at trace level using photoacoustic spectroscopy in industrial and environmental applications, Spectrochim. Acta A Mol. Biomol. Spectrosc. 60 (14) (2004) 3259–3268, http://dx.doi.org/10.1016/j.saa.2003.11.032.

[5] Y.V. Kistenev, A.V. Borisov, D.A. Kuzmin, O.V. Penkova, N.Y. Kostyukova, A.A. Karapuzikov, Exhaled air analysis using wideband wave number tuning range infrared laser photoacoustic spectroscopy, J. Biomed. Opt. 22 (1) (2017) 017002, http://dx.doi.org/10.1117/1.JBO.22.1.017002.

[6] A. Sampaolo, P. Patimisco, M. Giglio, A. Zifarelli, H. Wu, L. Dong, V. Spagnolo, Quartz-enhanced photoacoustic spectroscopy for multi-gas detection: A review, Anal. Chim. Acta 1202 (2022) 338894, http://dx.doi.org/10.1016/j.aca.2021.338894, URL https://www.sciencedirect.com/science/article/pii/S0003267021007200.

[7] N.Y. Kostyukova, A.A. Boyko, V. Badikov, D. Badikov, G. Shevyrdyaeva, V. Panyutin, G.M. Marchev, D.B. Kolker, V. Petrov, Widely tunable in the mid-IR $BaGa_4Se_7$ optical parametric oscillator pumped at 1064 nm, Opt. Lett. 41 (15) (2016) 3667–3670, http://dx.doi.org/10.1364/OL.41.003667, URL https://opg.optica.org/ol/abstract.cfm?URI=ol-41-15-3667.

[8] K.L. Vodopyanov, I. Makasyuk, P.G. Schunemann, Grating tunable 4 - 14 μm GaAs optical parametric oscillator pumped at 3 μm, Opt. Express 22 (4) (2014) 4131–4136, http://dx.doi.org/10.1364/OE.22.004131, URL https://opg.optica.org/oe/abstract.cfm?URI=oe-22-4-4131.

[9] A.A. Karapuzikov, I. Sherstov, D.B. Kolker, A.I. Karapuzikov, Y. Kistenev, D.A. Kuzmin, M.Y. Shtyrov, N.Y. Dukhovnikova, K.G. Zenov, A.A. Boyko, M.K. Starikova, I.I. Tikhonyuk, I.B. Miroshnichenko, M.B. Miroshnichenko, Y.B. Myakishev, V.N. Lokonov, LaserBreeze gas analyzer for noninvasive diagnostics of air exhaled by patients, Phys. Wave Phenomena 22 (3) (2014) 189–196, http://dx.doi.org/10.3103/S1541308X14030054.

[10] Y.V. Kistenev, A.V. Borisov, A.V. Shapovalov, O.Y. Nikiforova, Analysis of the component composition of exhaled air using laser spectroscopy and canonical correlation analysis, in: O.A. Romanovskii (Ed.), 21st International Symposium Atmospheric and Ocean Optics: Atmospheric Physics, in: Society of Photo-Optical Instrumentation Engineers (SPIE) Conference Series, vol. 9680, 2015, p. 96804C, http://dx.doi.org/10.1117/12.2205786.

[11] F.J. Harren, S.M. Cristescu, Photoacoustic spectroscopy in trace gas monitoring, in: Encyclopedia of Analytical Chemistry, John Wiley & Sons, Ltd, 2019, pp. 1–29, http://dx.doi.org/10.1002/9780470027318.a0718.pub3.

[12] M. Niu, Q. Liu, K. Liu, Y. Yuan, X. Gao, Temperature-dependent photoacoustic spectroscopy with a T shaped photoacoustic cell at low temperature, Opt. Commun. 287 (2013) 180–186, http://dx.doi.org/10.1016/j.optcom.2012.09.023, URL https://www.sciencedirect.com/science/article/pii/S0030401812010000.

[13] M. Krstic, I. Kanellakopoulos, P. Kokotovic, Nonlinear and Adaptive Control Design, A Wiley-Interscience Publication, Wiley, 1995, URL https://books.google.ru/books?id=wxkoAQAAMAAJ.

[14] Discrete time extremum seeking, in: Real-Time Optimization By Extremum-Seeking Control, John Wiley & Sons, Ltd, 2003, pp. 61–70, http://dx.doi.org/10.1002/0471669784.ch4, arXiv:https://onlinelibrary.wiley.com/doi/pdf/10.1002/0471669784.ch4, URL https://onlinelibrary.wiley.com/doi/abs/10.1002/0471669784.ch4.

[15] S.L. Brunton, C.W. Rowley, S.R. Kulkarni, C. Clarkson, Maximum power point tracking for photovoltaic optimization using ripple-based extremum seeking control, IEEE Trans. Power Electron. 25 (10) (2010) 2531–2540, http://dx.doi.org/10.1109/TPEL.2010.2049747.

[16] S.L. Brunton, X. Fu, J.N. Kutz, Extremum-seeking control of a mode-locked laser, IEEE J. Quantum Electron. 49 (10) (2013) 852–861, http://dx.doi.org/10.1109/JQE.2013.2280181.

[17] J.N. Kutz, S.L. Brunton, Intelligent systems for stabilizing mode-locked lasers and frequency combs: Machine learning and equation-free control paradigms for self-tuning optics, Nanophotonics 4 (4) (2015) 459–471, http://dx.doi.org/10.1515/nanoph-2015-0024.

[18] V.A. Sherstov, A.M. Goncharenko, K.G. Zenov, R.V. Pustovalova, A.I. Karapuzikov, Method for measuring the resonant frequency of photoacoustic detector in the real-time mode, Instrum. Exp. Tech. 59 (5) (2016) 749–753, http://dx.doi.org/10.1134/S0020441216050079.

[19] D.B. Kolker, A.A. Boyko, N.Y. Dukhovnikova, K.G. Zenov, I.V. Sherstov, M.K. Starikova, I.B. Miroshnichenko, M.B. Miroshnichenko, D.A. Kashtanov, I.B. Kuznetsova, M.Y. Shtyrov, S. Zachariadis, A.I. Karapuzikov, A.A. Karapuzikov, V.N. Lokonov, Continuously wavelength tuned optical parametric oscillator based on fan-out periodically poled lithium niobate, Instrum. Exp. Tech. 57 (2014) 50–54, http://dx.doi.org/10.1134/S0020441214010217.

[20] S.L. Brunton, J.N. Kutz, Data Driven Science & Engineering: Machine Learning, Dynamical Systems, and Control, Cambridge Textbook, 2019.

[21] D. MacDougall, W.B. Crummett, et al., Guidelines for data acquisition and data quality evaluation in environmental chemistry, Anal. Chem. 52 (14) (1980) 0003–2700, http://dx.doi.org/10.1021/ac50064a004.